Clusters and Shell-Structure in Light Nuclei

Thomas Neff*, Hans Feldmeier* and Robert Roth†

*Gesellschaft für Schwerionenforschung mbH, Planckstraße 1, 64291 Darmstadt, Germany
†Institut für Kernphysik, TU Darmstadt, Schlossgartenstraße 9, 64289 Darmstadt, Germany

Abstract. Light nuclei in the *p*-shell are studied in the Fermionic Molecular Dynamics model. No a priori assumptions are made with respect to cluster structure or single-particle energies. The same effective interaction based on the Argonne V18 interaction is used for all nuclei. Short-range central and tensor correlations are treated explicitly using a unitary correlation operator. Calculations of binding energies and radii for Helium and Carbon isotopes are presented. The evolution of cluster and single-particle structures with increasing neutron number are discussed. The spectrum of ^{12}C is calculated in a multiconfiguration calculation. The molecular structure of the excited states is investigated.

FERMIONIC MOLECULAR DYNAMICS

The A-body basis states in Fermionic Molecular Dynamics [1] are parity and angular momentum projected Slater determinants $\left|\, Q \,\right\rangle$

$$\left|\, Q^{J^\pi}_{MK} \,\right\rangle = P^{J^\pi}_{MK} \left|\, Q \,\right\rangle \tag{1}$$

of single particle states $\left|\, q_i \,\right\rangle$

$$\left|\, Q \,\right\rangle = \mathscr{A} \left\{ \left|\, q_1 \,\right\rangle \otimes \ldots \otimes \left|\, q_A \,\right\rangle \right\} . \tag{2}$$

The single-particle wave functions are described by Gaussian wave packets localized in phase-space

$$\left\langle\, \mathbf{x} \,\middle|\, q \,\right\rangle = \sum_i c_i \exp\left\{ -\frac{(\mathbf{x}-\mathbf{b}_i)^2}{2a_i} \right\} \left|\, \chi_i \,\right\rangle \otimes \left|\, \xi \,\right\rangle . \tag{3}$$

Whereas the AMD approach [2] uses a common width parameter a for all the wave packets the FMD treats the width as a complex variational parameter that can be different for each wave-packet. Also the spins $\left|\, \chi \,\right\rangle$ of each wave packet are treated as variational parameters. A superposition of two Gaussian wave packets is used for each single-particle state $\left|\, q_i \,\right\rangle$.

The basic FMD many-particle state is determined by minimizing the intrinsic energy of the parity projected Slater determinant

$$E\left[\left|\, Q^\pi \,\right\rangle\right] = \frac{\left\langle\, Q^\pi \,\middle|\, H_{eff} - T_{cm} \,\middle|\, Q^\pi \,\right\rangle}{\left\langle\, Q^\pi \,\middle|\, Q^\pi \,\right\rangle} \tag{4}$$

with respect to the parameters of all single-particle states. The projection on angular momentum eigenstates is done after the minimization. The obtained correlation energies can be very large for the often deformed and clustered nuclei in the *p*-shell. We therefore improve this projection after variation procedure (PAV$^\pi$) by implementing a variation after projection (VAP) procedure in the sense of the generator coordinate method (GCM). We minimize the energy of the Slater determinants under additional constraints on collective variables like radius, dipole, quadrupole or octupole moments. The VAP minimum can then be found by minimizing the projected energies with respect to the constraints. A further improvement is achieved by diagonalizing the Hamiltonian in a set of many-body states. This allows to study also excited states.

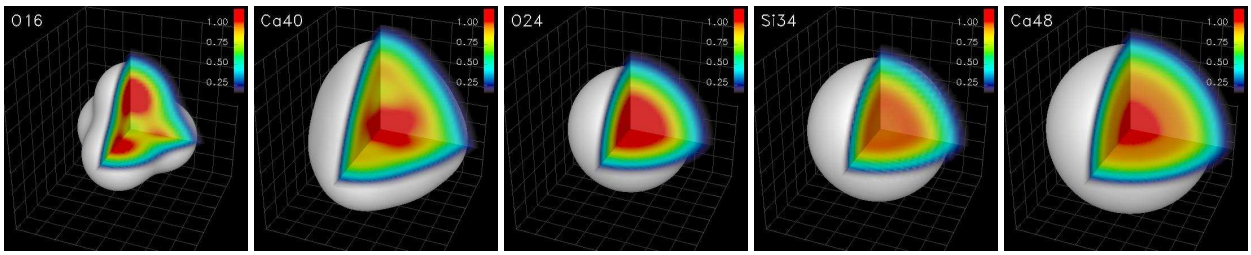

FIGURE 1. The correction term of the effective interaction is fitted to tetrahedral ^{16}O and ^{40}Ca configurations. The intrinsic energies of the tetrahedral configurations are about 10 MeV higher than that of the spherical configurations. After angular momentum projection they are about 5 MeV lower in energy. In case of ^{24}O, ^{34}Si and ^{48}Ca we find spherical configurations.

EFFECTIVE INTERACTION

For our calculations we use an effective interaction that is derived from the realistic Argonne V18 interaction by means of the Unitary Correlation Operator Method (UCOM) [3, 4, 5]. The correlated interaction includes the short-range central and tensor correlations induced by the repulsive core and the tensor force. The correlated interaction is very similar to the $V_{low\,k}$ [9] and no longer connects to high momenta. Thus it can be used directly with simple many-body states of a Hartree-Fock or FMD approach. The missing contributions of three-body correlations and genuine three-body forces are simulated by an additional two-body correction term. This correction term consists of a central momentum dependent part that is adjusted to fix the saturation properties by fitting to the binding energies and radii of ^{4}He, ^{16}O, ^{40}Ca and an isospin dependent spin-orbit term that is fitted to the binding energies of ^{24}O, ^{34}Si and ^{48}Ca. The correction term used in this paper differs slightly from the one in [5] as ^{16}O and ^{40}Ca are considered as tetrahedral α-cluster states that are about 5 MeV lower in energy after angular momentum projection than the spherical configurations (see Fig. 1). Altogether the correction term contributes about 15% to the total potential energy.

When minimizing the energy we often find that the intrinsic structure obtained depends strongly on the strength of the spin-orbit force. A strong spin-orbit force generally prefers closed shell configurations whereas a weak spin-orbit force often prefers more clustered configurations. The correlation energy obtained by parity and angular momentum projection is in general significantly greater for clustered configurations. For this reasons we find the strength of the spin-orbit force to be a useful generator coordinate. We generate configurations with interactions that differ in the strength of the spin-orbit force. The final energy is of course always calculated with the same fixed spin-orbit force.

HELIUM ISOTOPES

Fig. 2 shows the intrinsic states obtained by minimizing the energy of the Helium isotopes. In all nuclei a dipole deformation caused by a displacement of the neutrons against the α-core is found. In ^{6}He the configuration with two neutrons on the same side of the core is preferred to configurations with the two neutrons located at opposite sides

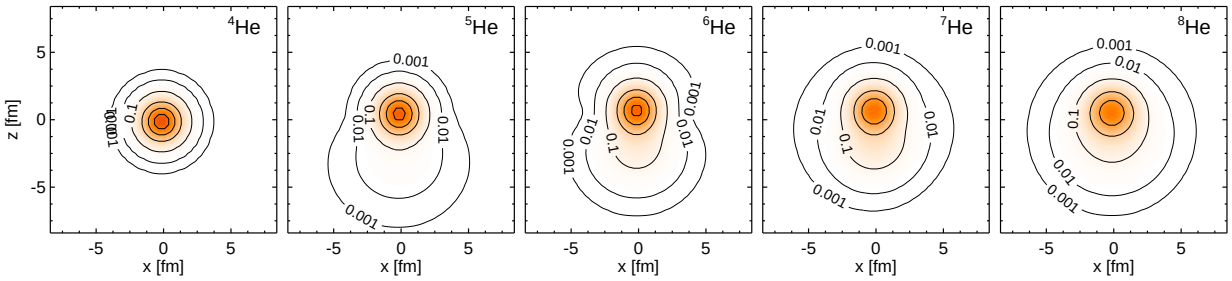

FIGURE 2. Intrinsic shapes of Helium isotopes corresponding to the minima in a variation after parity projection (PAV$^\pi$) calculation. Shown are cuts through the nucleon density calculated with the intrinsic state before parity projection. Densities are given in units of nuclear matter density $\rho_0 = 0.17\text{fm}^{-3}$.

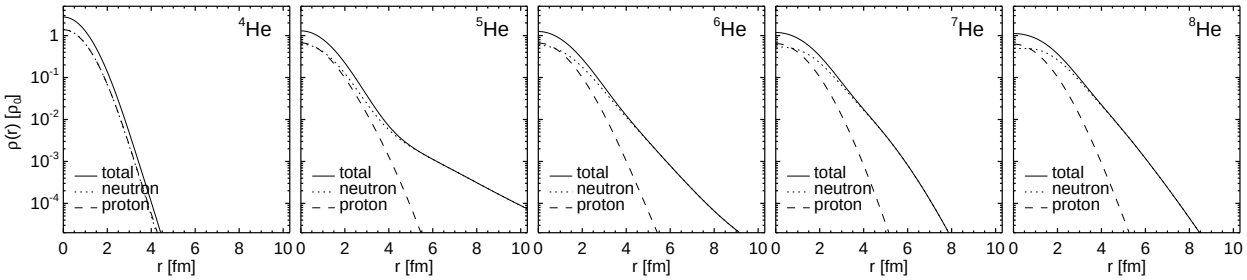

FIGURE 3. Radial density distributions for the Helium isotopes using angular momentum projected multiconfiguration states. The center of mass motion has been removed.

of the core. In ^{8}He one approaches the $p_{3/2}$ neutron shell closure with an almost spherical neutron distribution. In Fig. 4 the binding energies and matter radii obtained after angular momentum projection (PAV$^{\pi}$) are compared to the experimental binding energies and radii. To improve the many-body states we create additional configurations using the dipole moment as a generator coordinate. The multiconfiguration calculations reproduce the experimental binding energies and radii very well. This illustrates the importance of the soft-dipole mode, that is realized in the form of groundstate correlations, for the understanding of the borromean nature of ^{6}He and ^{8}He. Besides the neutron halo we can see the broadened proton distribution that is caused by the motion of the α core against the center of mass of the nucleus. For ^{6}He we calculate a charge radius of 2.02 fm that has to be compared to the recently measured value of 2.054 ± 0.014 fm [7].

In case of the resonances ^{5}He and ^{7}He one expects significant contributions from ^{4}He plus neutron or ^{6}He plus neutron cluster states. The ^{4}He core of ^{5}He is well described by a single Slater determinant but for a proper description of ^{7}He an angular momentum projected ^{6}He core would be needed.

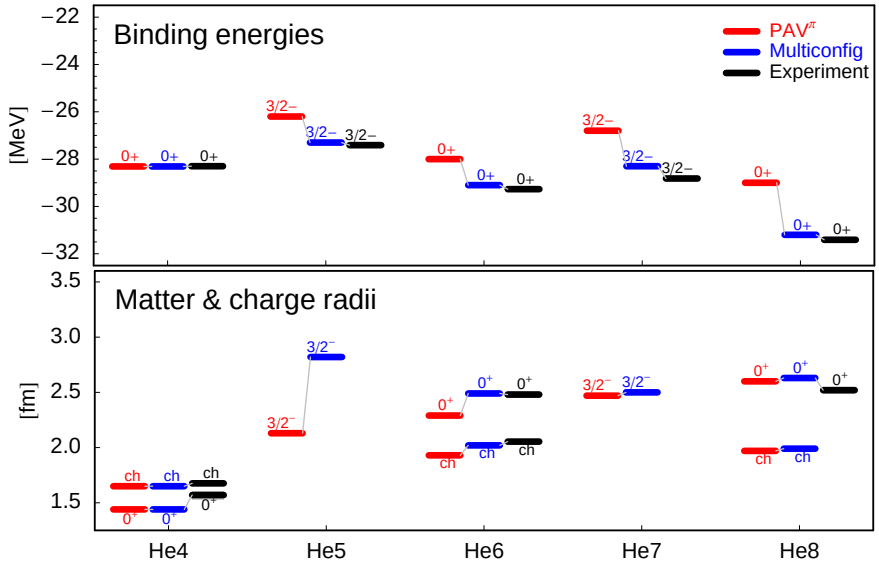

FIGURE 4. Binding energies and matter and charge radii for the Helium isotopes. Charge radii are indicated by ch. Results are given for the PAV$^{\pi}$ and the multiconfiguration calculations. Experimental matter radii are taken from [6]. The experimental charge radius of ^{6}He is given in [7].

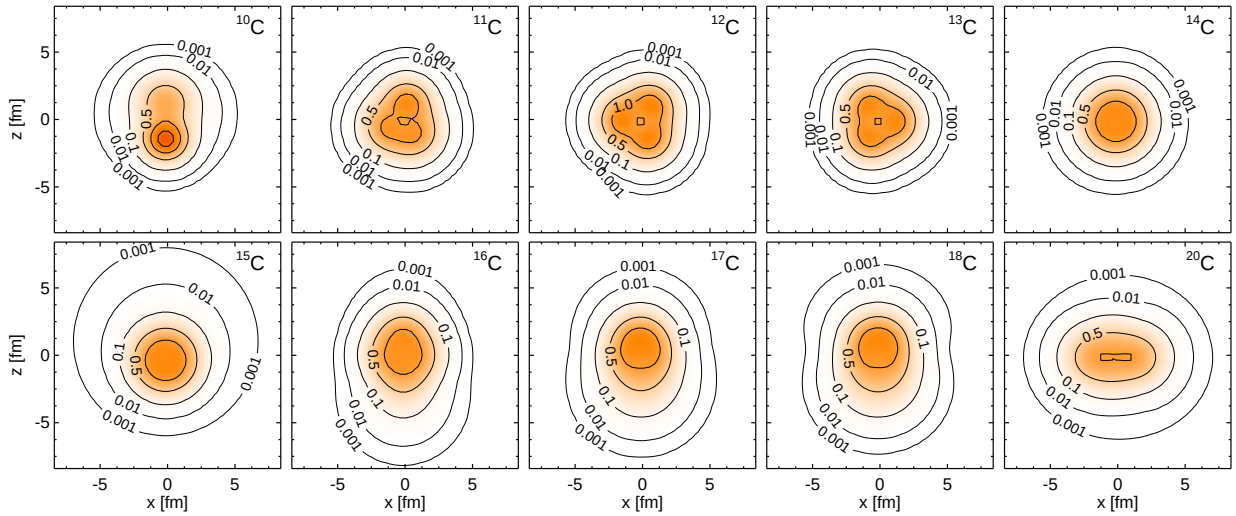

FIGURE 5. Intrinsic densities of Carbon isotopes corresponding to the variation after parity projection minima.

CARBON ISOTOPES

In the Carbon isotopes we observe many different structures as can be seen in Fig. 5. We see a prolate ^{10}C and find oblate triangular structures in ^{11}C, ^{12}C and ^{13}C. In ^{14}C we find that the fully occupied neutron *p*-shell induces a spherical configuration. In ^{15}C the additional neutron occupies mainly a $1s_{1/2}$ state whereas the following isotopes from ^{16}C to ^{18}C show prolate deformations caused by filling up neutrons in the *sd*-shell. We also observe that the deformation is dominated by the neutrons. In Fig. 6 the proton and neutron densities of the intrinsic state of ^{16}C are shown. If we project out from this intrinsic state the 0^+ and 2^+ states and calculate the $B(E2)$ value for the $0^+ \rightarrow 2^+$ transition we obtain a value of $9.3\,e^2\text{fm}^4$ that has to be compared to the surprisingly small experimental value of $3.15 \pm 0.95\,e^2\text{fm}^4$ [8]. No effective charges are used for protons and neutrons and the electrical quadrupole moment is therefore directly connected to the polarized proton distribution. The reason for the smaller than expected $B(E2)$ value is in this picture caused by the decoupling of proton and neutron distributions.

When we compare the calculated with the experimental binding energies and radii (see Fig. 7) we find a very good agreement for the multiconfiguration calculations with the experimental binding energies. The binding energies obtained for the single Slater determinants of the PAV$^{\pi}$ approach are able to reproduce the evolution of the binding energies to the heavy isotopes. For ^{12}C to ^{14}C experimental charge radii are known and reproduced well by our calculations. For the matter radii we find significantly larger values for the lighter isotopes up to ^{14}C. There is some uncertainty in the experimental determination of the matter radii beyond the given error bars and as we find a good agreement of our calculated charge radii in this region there might be a problem with these experimental results. In case of ^{15}C our matter radius is much larger. This is probably explained by the very weak binding of the $1s_{1/2}$ neutron. Our calculated neutron separation energy of ^{15}C is too small, the *s*-orbit therefore much more extended. For the heavier

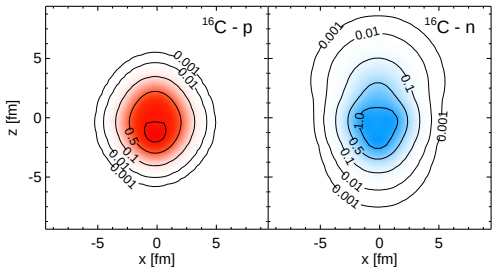

FIGURE 6. Proton (left) and neutron (right) densities of the ^{16}C intrinsic state obtained as the PAV$^{\pi}$minimum.

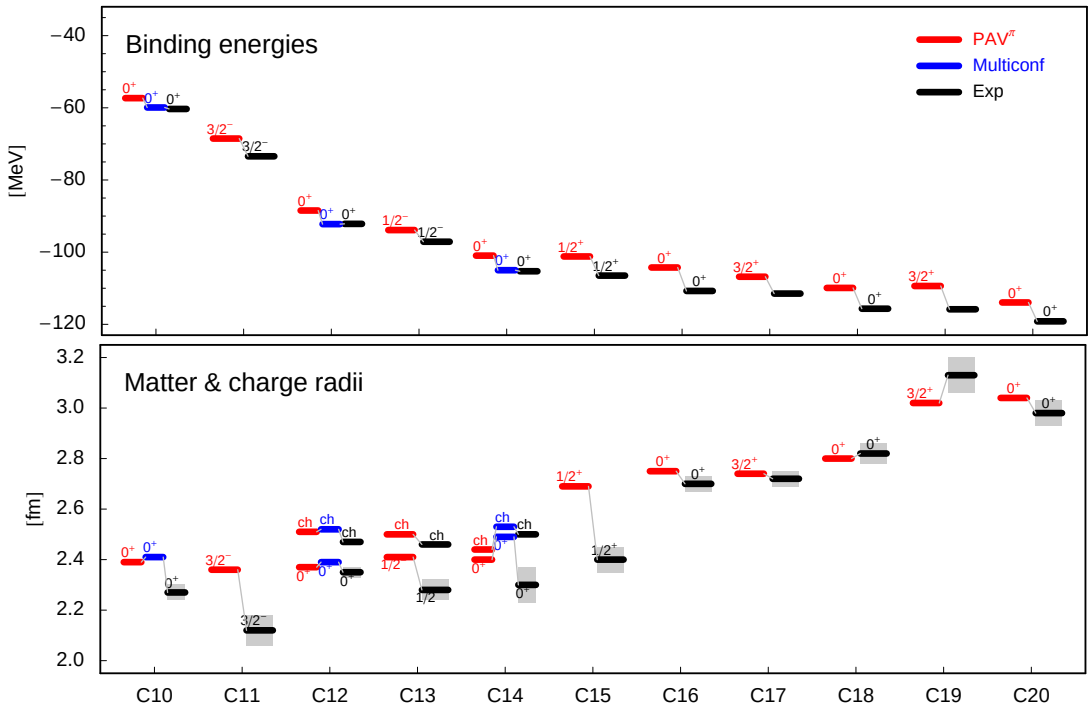

FIGURE 7. Energies and matter and charge radii of Carbon Isotopes. Calculated charge radii (indicated by ch) are only shown if experimental values are known. Multiconfiguration calculations have only been done for ^{10}C, ^{12}C and ^{14}C.

isotopes the calculated matter radii agree well with experimental values.

^{12}C SPECTRUM

The structure of ^{12}C is characterized by an interplay between shell-model and cluster structure. If we perform an unconstrained minimization of the energy we end up with a spherical ^{12}C that is identical to the $(0s_{1/2})^4(0p_{3/2})^8$ shell model configuration. The energy for this configuration is about 10 MeV too high compared to experiment and the radius is too small (see Tab. 1). If we try a Brink type α-cluster wave function we find a configuration that has a similar energy but a radius much larger than experiment. Whereas in the shell model configuration the spin-orbit interaction contributes strongly to the binding energy, the α-cluster configuration has no contribution by the spin-orbit force. The α-cluster configuration on the other hand has a very big correlation energy due to the angular momentum projection. If we minimize after parity projection (PAV$^\pi$) or search for the variation after projection minimum (VAP using the radius and the octupole moment as constraints) we find solutions that are significantly lower in energy. In these configurations the spin-orbit and correlation energy contributions are somewhere in between the pure shell model

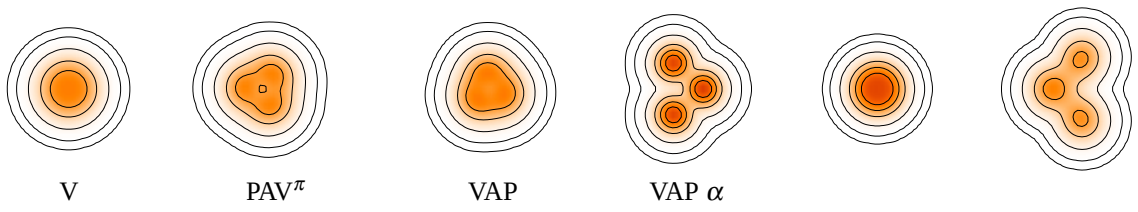

FIGURE 8. Intrinsic shapes of ^{12}C corresponding to the variation (V), the variation after parity projection (PAV$^\pi$), the variation after angular momentum projection (VAP) and the variation after projection for a Brink α-cluster trial state (VAP α). The four right most configurations are used for the Multiconfig(4) calculation.

TABLE 1. Binding energies, radii and $B(E2)$ transition strength calculated with FMD states.

	$\mathbf{E_b}$ [MeV]	$\mathbf{r}_{charge}$ [fm]	$\mathbf{B(E2)}$ [e^2fm^4]
V/PAV	81.4	2.36	-
VAP α-cluster	79.1	2.70	76.9
PAV$^\pi$	88.5	2.51	36.3
VAP	89.2	2.42	26.8
Multiconfig (4)	92.2	2.52	42.8
Multiconfig (14)	92.4	2.52	42.9
Experiment	92.2	2.47	39.7 ± 3.3

and α cluster configurations.

The angular momentum projection of the PAV$^\pi$solution already provides a reasonable description of the groundstate rotational band of ^{12}C. We can improve this description by performing a multiconfiguration calculation with four intrinsic states. Starting with the VAP configuration we consecutively add configurations that improve the groundstate energy. In the Multifonfig(4) calculation the groundstate rotational band including the $B(E2)$ transition strength for the $0^+ \rightarrow 2^+$ transition is well reproduced. In addition we find a second 0^+ state, the famous Hoyle state. A description of this state as a Bose condensate of α particles has been proposed[10]. We improve our many-body basis by creating 10 additional α-cluster configurations using quadrupole and octupole moments as constraints. The resulting Multiconfig(14) result is displayed in Fig. 9 indicating a significant improvement of the 0^+_2 energy. We obtain a monopole matrix element for the $0^+_1 \rightarrow 0^+_2$ transition of $5.67\,\mathrm{fm}^2$ that has to be compared with the experimental value of $(5.5 \pm 0.2)\,\mathrm{fm}^2$.

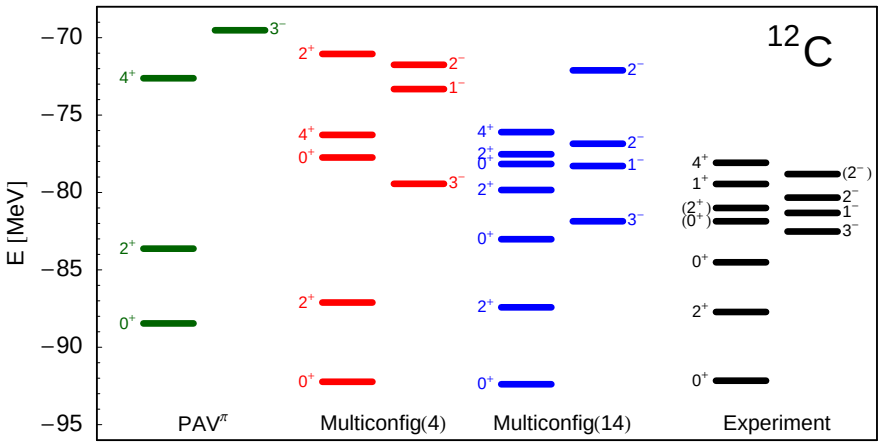

FIGURE 9. Spectrum of ^{12}C calculated using the single intrinsic state obtained in the variation after parity projection calculation (PAV$^\pi$) and in multiconfiguration calculations using 4 and 14 Slater determinants. The experimental spectrum is shown for comparison.

REFERENCES

1. H. Feldmeier and J. Schnack, *Rev. Mod. Phys.* **72** (2000) 655. and references therein
2. Y. Kanada-En'yo and H. Horiuchi, *Prog. Theor. Phys. Suppl.* **142** (2001) 205
3. H. Feldmeier, T. Neff, R. Roth, J. Schnack, *Nuc. Phys.* **A632** (1998) 61
4. T. Neff and H. Feldmeier, *Nuc. Phys.* **A713** (2003) 311
5. R. Roth, T. Neff, H. Hergert, H. Feldmeier, `nucl-th/0406021`, to appear in *Nuc. Phys.* **A**
6. A. Ozawa, T. Suzuki, I. Tannihata, *Nuc. Phys.* **A693** (2001) 32
7. L.-B. Wang et al, *Phys. Rev. Lett* **93** (2004) 142501
8. N. Imai et al, *Phys. Rev. Lett.* **92** (2004) 062501
9. S.K. Bogner, T.T.S. Kuo and A. Schwenk, *Phys. Rept.* **386** (2003) 1
10. Y. Funaki, A. Tohsaki, H. Horiuchi, P. Schuck and G. Röpke, *Phys. Rev.* **C67** (2003) 051306